Inorganic Chemistry

Article

pubs.acs.org/IC

Water Vapor Diffusion into a Nanostructured Iron Oxyhydroxide

Xiaowei Song* and Jean-François Boily

Department of Chemistry, Umeå University, SE-901 87 Umeå, Sweden

Supporting Information

ABSTRACT: Water diffusion through 0.4 nm × 0.4 nm wide tunnels of synthesized akaganéite (β-FeOOH) nanoparticles was studied by a coupled experimental−molecular modeling approach. A sorption isotherm model obtained from quartz crystal microbalance measurements suggests that the akaganéite bulk can accommodate a maximum of 22.4 mg of water/g (44% bulk site occupancy) when exposed to atmospheres of up to 16 Torr water vapor. Fourier transform infrared spectroscopy also showed that water molecules interact with (hydr)oxo groups on both the akaganéite bulk and surface. Diffusion reactions through the akaganéite bulk were confirmed through important changes in the hydrogen-bonding environment of bulk hydroxyl groups. Molecular dynamics simulations showed that water molecules are localized in cavities that are bound by eight hydroxyl groups, forming short-lived (<0.5 ps) hydrogen bonds with one another. Diffusion coefficients of water are three orders of magnitude lower than they are in liquid water (D = 0.0−11.1 × 10^{-12} $m^2 \cdot s^{-1}$), whereas large integral rotational correlation times are 4 to 15 times higher (τ_r = 8.4−31.8 ps). Moreover, both of these properties are strongly loading-dependent. The simulations of the interface between the water vapor phase and the (010) surface plane of the akaganéite, where tunnel openings are exposed, revealed sluggish rates of incorporation between interfacial water species and their tunnel counterparts. The presence of defects in the synthesized particles are suspected to contribute to different diffusion rates in the laboratory when compared to those observed in pristine crystalline materials, as studied by molecular modeling.

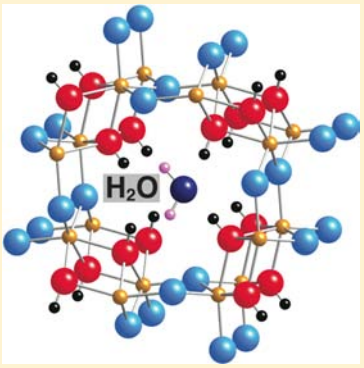

1. INTRODUCTION

Akaganéite (β-FeOOH·$(HCl)_{0.11-0.19}$)[1−3] is an iron oxyhydroxide mineral with a hollandite-type structure that consists of 0.4 nm × 0.4 nm wide tunnels[2] that are capable of exchanging with various ions and water molecules[2,4−6] from surrounding media (Figure 1). This mineral occurs naturally in chloride-rich environments, such as oceans, saline lakes, hot brines, mines, and soils[2,7−10] and can form from the oxidation of pyrrhotite ($Fe_{1-x}S_x$),[10] as, for example, in lunar samples brought back to earth from the Apollo mission.[11,12] Previous studies have speculated on its possible presence on Mars, where it might serve as a suitable sink for chloride and water.[13−16] A common corrosion product of steels,[17,18] it has also been used as an efficient and low-cost contaminant sorbent.[19−21] It also has potential uses in lithium iron cells[22,23] as well as in the fabrication of magnetic nanocapsules for pharmaceutical drug delivery.[24] Although many of these various applications take advantage of akaganéite's nanostructured tunnels and large specific surface area, its exchange mechanisms with water-bearing environments have not been sufficiently well-resolved.

Akaganéite particles are typically nanosized and acicular in shape with exposed tunnel openings at the terminations of the particles that we represent here as the (010) plane (Figure 1a).[1−3,25] These openings (~0.16 nm^2) are the predominant ports of entry for ions and water molecules that diffuse throughout the length of the particles.[3−5,26] Typical akaganéite samples that are equilibrated under circumneutral aqueous conditions have 60−75%[27] of their unit cells occupied by Cl^-.[2] Various studies have shown that akaganéite can incorporate other monovalent ions (e.g., F^-, Br^-, and OH^-)[4,5,28] but not larger moieties, such as phenyl rings or perchlorate.[27] In a previous study from our group, we also noticed the presence of a Cl^- pool on akaganéite surfaces that can be exchanged and released into aqueous solutions by stronger binding ligands (e.g., SO_4^{2-}) and that later codiffuse with protons within the akaganéite tunnels.[27] There, chloride ions (ionic radius = 0.18 nm)[29] can be stabilized by hydrogen bonds from eight surrounding bulk OH groups (Figure 1b). These interactions red shift the bulk OH vibrational-stretching frequencies, expand the crystal lattice size, and increase the thermal stabilities of this material.[26]

Recent calorimetric[5] and thermogravimetric analysis studies[30,31] of akaganéite have discussed the possibilities for the presence of bulk water. Water can diffuse through akaganéite's tunneled structure because of its size (H_2O radius = 0.14 nm)[32] and its ability to both donate and accept hydrogen bonds (Figure 1c). Given the multiple uses for akaganéite and its interesting potential for encapsulating water possibly in Martian[33] soils, a detailed understanding of the nature of the bulk occluded water is required. This study therefore addresses this issue by reporting the water uptake capacity and the plausible molecular structures that are adopted in synthesized akaganéite nanoparticles. The quartz crystal microbalance (QCM) method was used to determine the water uptake capacity, and Fourier transform infrared (FTIR) spectroscopy

Received: March 18, 2013
Published: May 23, 2013

   dx.doi.org/10.1021/ic400661d | *Inorg. Chem.* 2013, 52, 7107−7113

concomitantly probed how the hydrogen-bonding environment of the akaganéite bulk was affected by water diffusion. Finally, molecular dynamics (MD) simulations elucidated the mechanisms by which water diffusion reactions proceed from the akaganéite surface to its bulk.

2. EXPERIMENTAL SECTION

2.1. Akaganéite Synthesis. The particles were synthesized by the hydrolysis of a $FeCl_3$ solution in CO_2-free aqueous media,[34] as detailed in the Supporting Information (SI). All of the solids were dialyzed with preboiled, N_2(g)-degassed deionized water (18.2 MΩ·cm). The structural and chemical characterizations of these particles are reported in the SI. Briefly, the particles are acicular in shape and monodispersed in size with dimensions of 7−11 nm in the *a* and *c* crystallographic directions and 80−110 nm in *b* (Figure 1). The transmission electron images can be found in Figure 2 and in Song and Boily.[26] On the basis of the crystal habits of the particles, the dominant surfaces were deemed to consist of the isostructural (100) and (001) planes, accounting for 95% of the total area.[35] The terminal (010) plane accounts for the remaining 5% of the surface area. The N_2(g) BET specific surface area[35] (111.2 m^2/g) falls on the lower end (110−160 m^2/g) of the values that were calculated from the particle sizes using a specific gravity of 3.73 g/cm^3. The goethite and lepidocrocite particles that were used in this work were the same samples from our previous studies.[36]

2.2. Fourier Transform Infrared Spectroscopy. Wet pastes obtained by centrifugation of the mineral suspensions were transferred onto a fine tungsten mesh (Unique Wire Weaving, 0.002 in. mesh diameter), squeezed into a copper sample holder, and dried into a thin film under N_2(g) flow overnight. The water vapor sorption experiments were then carried out on the dry mineral films in a vacuum cell (AABSPEC no. 2000-A) that was equipped with KBr windows. The different loading of H_2O was introduced into the samples by a flow of carrier N_2(g). CO_2-free water vapor was generated by passing dry N_2(g) through an airtight water bath to produce moist N_2(g). This moist flow was then mixed with dry N_2(g) at ratios that were controlled by mass-flow controllers (MKS, 179A) while maintaining the total flow rate at 200 standard cubic centimeters per minute (SCCM). For each loading, the water vapor was equilibrated with the sample for 20 minutes. Water vapor levels were monitored using a nondispersive infrared analyzer (LI-7000, Licor, Inc.).

FTIR spectra were collected in situ with a Bruker Vertex 70/V FTIR spectrometer equipped with a DLaTGS detector. All of the spectra were collected in the 600−4500 cm^{-1} range at a resolution of 4.0 cm^{-1} and at a forward/reverse scanning rate of 10 Hz. The background spectra were obtained in vacuo for the same tungsten mesh that was used for the mineral−water experiments. Each spectrum was an average of 50 scans. Several numerical treatment procedures were applied to the raw spectra to obtain the spectral features. First, the contributions from gaseous (unadsorbed) water were removed using a previously developed chemometric model[37] that predicted the water vapor spectra to be in the 0−19 Torr range. The single value decomposition[38] (SVD) technique was thereafter applied to these spectra to remove random noise and error. Finally, FTIR-derived water sorption isotherms were obtained from the integrated band area of the water O−H bending region and beyond (1800−1400 cm^{-1}). These values were normalized with respect to the maximum amount of water uptake that was measured by dynamic vapor sorption experiments and will be discussed in the following section. All of the calculations were performed with MATLAB 7.0 (The Mathworks, Inc.).

2.3. Dynamic Vapor Sorption. A quartz crystal microbalance (QCM; eQCM 10M, Gamry Instruments, Inc.) was used to measure the water vapor uptake by the synthesized FeOOH minerals using the dynamic vapor sorption method. These experiments were not only carried out on akaganéite, but also on both the synthesized goethite (55.6 m^2/g) and lepidocrocite (64.4 m^2/g) that had been used in previous studies from our group.[36] The object of this experiment was to compare the amounts of water vapor adsorbed on FeOOH minerals that cannot allow water diffusion to the bulk (lepidocrocite and goethite) to that of akaganéite.

The mineral particles were deposited on the quartz crystal (10 MHz Au-coated) and dried under a 200 SCCM N_2(g) flow overnight into thin films. Before introducing the water, the mass of each sample was measured by QCM to certify that the sample was completely dry and that it had a constant, time-independent mass. The same mixed flows were used as in the FTIR experiments and were passed through the dry samples using a flow cell (CH Instruments, Inc.). A 20 min equilibrating period (Figure S1) was allowed for each water loading, during which time the end-flow water vapor levels were measured by a nondispersive infrared analyzer (LI-7000, LI-COR, Inc.). The frequency of the quartz resonator was continuously measured. The change in frequency was converted to a change in mass on the quartz crystal using the Sauerbrey equation.[39]

All QCM data were modeled using a modified expression of the Do−Do[40] water sorption isotherm:

$$C_\mu = C_{\mu s}\frac{K_\mu \sum_1^{n=\alpha+1} x^n}{K_\mu \sum_1^{n=\alpha+1} x^n + K_\mu \sum_1^{n=\alpha+1} x^{n-\alpha 1}} + S_o\frac{K_f \sum_1^{n=\beta+1} n x^n}{1 + K_f \sum_1^{n=\beta+1} x^n} + C_{\mu B} \quad (1)$$

The first term of this equation accounts for condensation, the second, for adsorption reactions, and the third, for bulk water molecules. The parameters for the condensation include the saturation concentration ($C_{\mu\sigma}$), the association constant (K_μ), and the number of molecules in the water cluster (α). The parameters for the adsorption include total crystallographic densities of (hydr)oxo groups on the akaganéite (S_o = 15.2 sites/nm^2), goethite (S_o = 15.2 sites/nm^2), and lepidocrocite surfaces (S_o = 12.8 sites/nm^2),[41,42] the association constant (K_f), and the number of hydration waters per site (β). Finally, the bulk water loading ($C_{\mu s}$) holds for akaganéite only ($C_{\mu s}$ = 0 in goethite and lepidocrocite). These parameters were co-optimized using a trust region reflective algorithm. All of the calculations were carried out in the computational environment of Matlab 7.0 (The Mathworks, Inc.).

2.4. Molecular Dynamics. MD simulations of the akaganéite bulk were carried out on neutrally charged $Fe_{1792}O_{1792}(OH)_{1792}$, $Fe_{1792}O_{1392}(OH)_{2192}Cl_{210}$, and $Fe_{1792}O_{1652}(OH)_{1932}Cl_{73}$ supercells starting from crystallographically determined dimensions of 4.235 nm × 4.244 nm × 4.206 nm.[1] The details of the procedures for how these cells were built were described previously.[26] Up to 367 simple point-charge (SPC) water molecules were thereafter inserted into these cells. Another cell, $Fe_{1664}O_{1152}(OH)_{1920}Cl_{202}$, was cut along the (010) plane and had dangling bonds that terminated with hydroxo groups. An 8 nm void containing 800 water molecules was placed in contact with this plane to simulate water vapor-like conditions. This void was also filled with 1 g/cm^3 water to simulate interactions with liquid water.

All of the cells were simulated by classical MD with a modified CLAYFF[43] force field and the flexible SPC[44] model for water. All of the parameter values and equations are reported in Table S1 of the SI. An NPT (constant number of particles, constant pressure, and constant temperature) ensemble with a time step of 0.5 fs for 5 ns (10^7 steps) simulations was used to integrate the equations of motion with the Verlet algorithm.[45] All of the production runs were preceded by a 5 ns simulation to pre-equilibrate the system. One simulation of the (010) plane was continued for ~6×10^8 steps (~600 ns, using a 1.0 fs time step) to monitor both the incorporation and diffusion of water from the surface into the akaganéite bulk. The initial 10^7 steps of this simulation were also reproduced using a 0.5 fs time step to ensure the compatibility between these approaches.

The temperature of the whole system (300 K) was coupled to the Nosé−Hoover velocity-rescale thermostat at a 0.1 ps relaxation time. The pressure (750.06 Torr) was coupled using an anisotropic scaling of the simulation box using the Parrinello−Rahman method.[46,47] The LINCS algorithm[48] was used to treat the O−H bonds of all hydroxyl

dx.doi.org/10.1021/ic400661d | Inorg. Chem. 2013, 52, 7107−7113

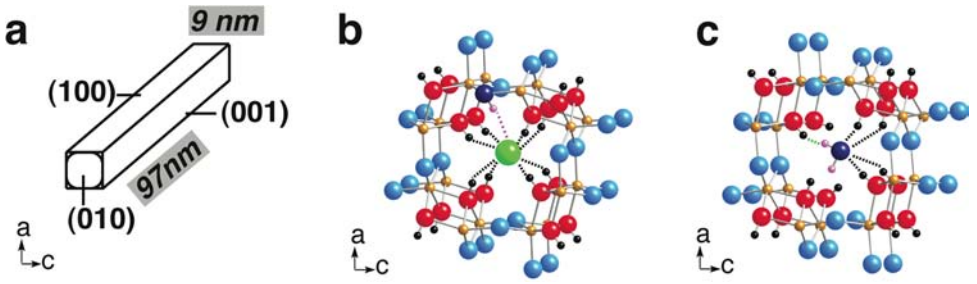

Figure 1. Particle morphology of akaganéite particles in which the tunnel openings are ideally exposed at the (010) plane (a). Tunnels containing chloride ion (b) or water (c). In Cl-occupied channels (b), an additional proton (pink) is present for charge balance. Dashed lines represent hydrogen bonds. (Fe, brown; bulk OH, red; bulk O, blue; and Cl^- ion, green.).

groups. A 0.8 nm cutoff was used for van der Waals interactions, and the particle mesh Ewald method[49,50] was used to treat long-range electrostatics. The power spectra were generated from the Fourier transform of the hydrogen velocity autocorrelation function obtained from 50 ps simulations performed with a 1.0 as time step (5×10^7 steps) by removing LINCS on O–H bonds. All of the calculations were carried out with Gromacs (v. 4.5.4).[51] The full details of the simulations are provided in the SI.

3. RESULTS AND DISCUSSION

Every unit cell of akaganéite (formula unit: 8·$FeOOH^2$) has one tunnel site where Cl^- can potentially be stored. The β-$FeOOH{\cdot}(Cl)_{0.25}$ composition represents the theoretically achievable maximum loading for this ion. The molecular dynamics simulations of water-bearing β-FeOOH cells (Figure 1c), to be further discussed in the latter part of this study, show that water sits at the same sites and can therefore yield the β-$FeOOH{\cdot}(H_2O)_{0.25}$ composition as the theoretical maximal water loading in this material as well. Thus, this composition amounts to a maximum of 50.6 mg of water/g of a hypothetically chloride-free and defect-free phase. In the following sections, water loadings on akaganéite will be monitored by QCM, whereas the nature of their interactions with bulk and surface hydroxo groups will be resolved using FTIR and MD.

3.1. Water Loading. Water loading on the dialyzed, synthesized nanoparticles greatly exceeded the β-$FeOOH{\cdot}(H_2O)_{0.25}$ composition (Figure 2) because these loadings arose from three distinct processes: (i) adsorption at particle surfaces, (ii) interparticle condensation, and (iii) diffusion to the akaganéite bulk. Water loading on the nanoparticles of two other synthesized FeOOH polymorphs[36] (goethite and lepidocrocite), which do not have nanostructured bulk interstices capable of incorporating water, are about half of those achieved by akaganéite below 13 Torr. In all of these three FeOOH phases, the adsorption reactions involved the hydration of surface (hydr)oxo groups and the subsequent accumulation of water layers. These are manifested by a strong uptake at low pressure, reaching a plateaulike feature above 2–4 Torr. The condensation reactions take place at larger pressures (10 Torr in akaganéite and 14 Torr in goethite and lepidocrocite) and are manifested by a sharp uptake of water. These latter reactions are facilitated in akaganéite, in contrast to the larger goethite and lepidocrocite, because of the tighter packing of these smaller particles. Adsorption and condensation reactions can be effectively predicted using the Do–Do[40] water adsorption isotherm model shown in Figure 2. The adsorption component of this model was constrained by the goethite and lepidocrocite data because of the strong similarity in both the

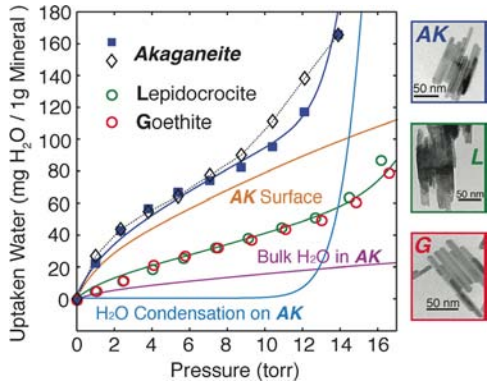

Figure 2. Water sorption isotherms of akaganéite (blue square), lepidocrocite (green circle), and goethite (red circle) obtained from dynamic vapor sorption experiments at 22 °C. Solid lines were generated using the Do–Do water vapor adsorption isotherm (eq 1) using optimized parameters as described in section 2.3. Adsorption (orange), condensation (light blue), and bulk diffusion (purple) components of the akaganéite model are also shown. The akaganéite isotherm data points (diamonds) were obtained from the integrated band areas of the water O–H bending region (Figure 4c) and normalized to the maximum amount of water measured by QCM. TEM images on the right show that these three FeOOH minerals are all acicularly shaped submicrometer-sized particles (scale bars = 50 nm).

surface site population and the density between these minerals and akaganéite.[35] By co-adjusting the condensation component of the modified Do–Do model (eq 1) with these data, a component for the diffusion to the bulk provided the model prediction shown in Figure 2. This model assumes concomitant water adsorption and diffusion throughout the 0–16 Torr range, with the latter resulting in a maximum of 22.4 mg of water/g in the akaganéite bulk. This value is within the theoretical maximum loading of 50.6 mg of water/g. Thus, this model points to a composition of $FeOOH{\cdot}(H_2O)_{0.11}$, namely, a 44% unit-cell occupancy for the synthesized particles. As the original dialyzed particles have a chloride occupancy of about 66% Cl^-, as shown in Song and Boily,[26] we expect that the large water loading may promote some exchange of HCl for water at the akaganéite particle surface where several layers of physisorbed water molecules have accumulated.

3.2. FTIR. Further evidence for water diffusion was detected by monitoring the hydrogen-bonding environment of the akaganéite surface and bulk OH groups using FTIR spectroscopy (Figures 3 and 4). The efforts in this work are notably focused on the O–H stretching region (~3800–3500 cm^{-1}) of the akaganéite surface hydroxo groups, providing evidence for

dx.doi.org/10.1021/ic400661d | Inorg. Chem. 2013, 52, 7107–7113

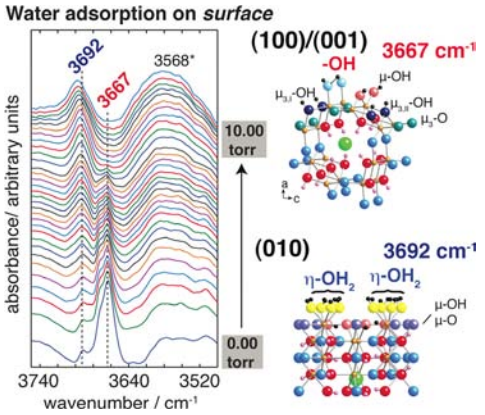

Figure 3. FTIR spectra of akaganéite particles exposed to gaseous water. Arrows denote intensity changes. Surface hydroxyl groups of the isostructural (100)/(001) planes and the terminal (010) plane are shown on the right. Dashed lines represent hydrogen bonds. (Fe, brown; bulk OH, red; bulk O, blue; and Cl^- ion, green.).

water adsorption reactions (Figure 3), and on the O−H stretching (~3600−2800 cm^{-1}) and bending regions of the akaganéite bulk (900−600 cm^{-1}) as well as that of water (1800−1400 cm^{-1}; Figure 4).

The narrow O−H stretching bands arising from the surface hydroxo groups on the dry particle surfaces were readily consumed by interactions with water, as notably seen by the loss of the 3667 cm^{-1} band (Figure 3) that corresponds to singly coordinated surface hydroxyls (−OH; ≡Fe−OH).[35] The strong attenuation and red shift of this band upon water loading was highly comparable to that which was already documented for lepidocrocite.[37] Just as in this mineral, this band was replaced by broader features below ~3600 cm^{-1} because of the formation of a network of hydrogen bonds that result from the accumulation of several water layers on the akaganéite surface. These hydrogen-bonded adsorbed water molecules display liquid-water-like spectral features at ~1640 cm^{-1}, shown in Figure 4c. The growth of the 3692 cm^{-1} band upon water loading is another prominent feature in these spectra (Figure 3). This band arises from the chemisorption of the water molecules onto bare Fe sites at the terminations of the akaganéite particles, namely, the (010) plane. The resulting complexes consist of geminal waters[35] (η-OH_2; ≡Fe-$(OH_2)_2$), illustrated in Figure 3, which are likely precursor species to those entering the akaganéite tunnel, as will be further detailed in section 3.3.

The evidence pointing to the diffusion within the akaganéite bulk was manifested by the different FTIR spectra of both the O−H stretching (Figure 4a,b) and bending (Figure 4c) regions of akaganéite and water. Other than the aforementioned surface groups (shown as negative peaks in Figure 4a), these spectra display a seemingly peculiar doublet that consists of bands at 3568 and 3227 cm^{-1}. This set of bands markedly contrasts with those of lepidocrocite and goethite in which a 3435 cm^{-1} band typically develops from liquidlike adsorbed water.[37] The appearance of this doublet can, however, be understood by recalling that the nanostructured tunnels of the akaganéite bulk are populated by OH groups that are donating hydrogen bonds to Cl^- ions (3410 cm^{-1}) as well as isolated (3485 cm^{-1}) counterparts (Figure 1b).[26] The water molecules that diffuse through the akaganéite bulk should thus preferentially interact with the isolated OH groups, thereby attenuating the spectral intensities near 3485 cm^{-1}. As these interactions broaden the range of O−H stretching frequencies for both OH and sorbed H_2O, the net effect of these interactions yields a rise in the intensity of the 3568/3227 cm^{-1} doublet and a sharp decline at 3516 cm^{-1} (Figure 4a). As additional support for this statement, the same phenomenon was observed for samples that were reacted with HCl (Figures S2 and S3). This concept can be substantiated further through the response of the Fe−O−H bending region (900−600 cm^{-1}) to water loading. This region specifically arises from both in-plane (795 cm^{-1}; a−c plane, perpendicular to the tunnel) and out-of-plane (673/623 cm^{-1}; along the tunnel) modes of vibration. Previous work[26] on HCl-reacted akaganéite showed that the incorporation of Cl^- strengthens in-plane bending but weakens out-of-plane bending because of hydrogen bonds that are formed with bulk OH groups. Exposing akaganéite to water vapor induces comparable features (Figure 4b) through both the shift of the in-plane 795 cm^{-1} band to the 850 cm^{-1} band and the shift of the out-of-plane 673/623 cm^{-1} band to 721/609 cm^{-1}.[26] The rise in the water-bending region (1640 cm^{-1}) is strongly correlated with these spectral changes. Finally, a sorption isotherm obtained from the integrated band area of this region (1400−1800 cm^{-1}) and normalized to the maximum water loading obtained by dynamic vapor deposition also corresponded remarkably well to the dynamic vapor sorption experiments (diamond symbols

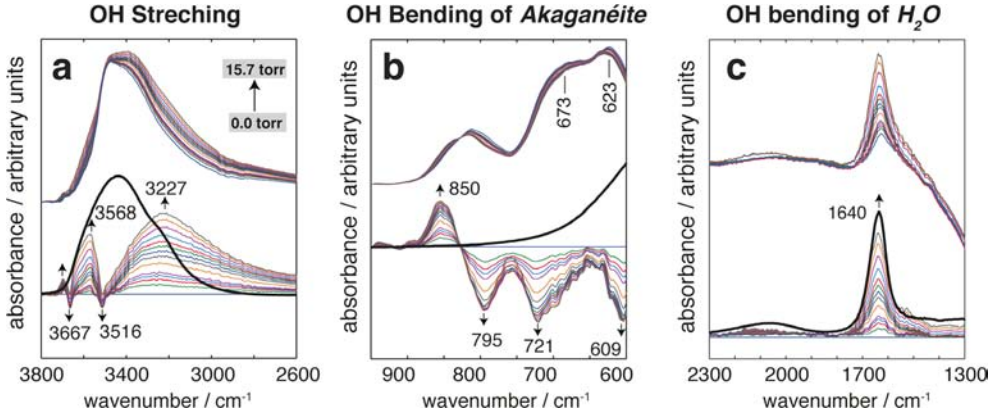

Figure 4. Stretching (a) and bending (b) modes of akaganéite particles that were exposed to 0.0−15.7 Torr gaseous water (top). The H_2O bending band is shown in panel c (top). Difference spectra (bottom) were obtained by subtracting the original mineral contribution from all spectra. The spectra of liquid water are shown in black line as a reference. Arrows denote intensity changes.

dx.doi.org/10.1021/ic400661d | Inorg. Chem. 2013, 52, 7107−7113

in Figure 2). This finding thereby provides a last piece of experimental evidence that supports the concept of simultaneously occurring water adsorption and diffusion reactions.

3.3. Water Uptake and Bulk Diffusion Mechanisms. The mechanisms of both water uptake by the akaganéite surface and the diffusion to its bulk were further elucidated by MD. The geminal waters at the (010) plane are the most energetically favorable adsorption centers for water vapor at loadings below the crystallographically available Fe sites. The resulting chemisorbed water molecules adopt a regular array of sites on this plane (Figure 5) that result from specific sets of

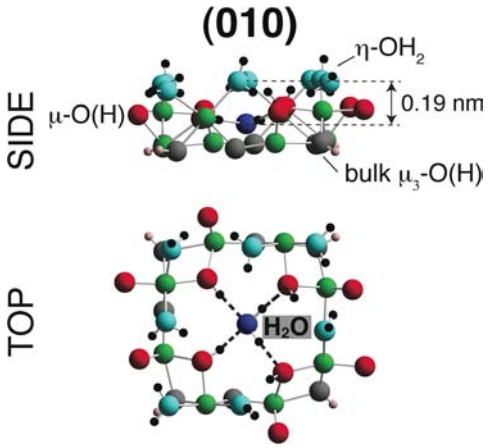

Figure 5. Schematic representation of water occupied in the unit cell tunnel structure of akaganéite showing the additional water species at the tunnel entrances just 0.19 nm below the geminal waters. Dashed lines represent hydrogen bonds. (Fe, green; η-OH_2, turquoise; μ-O(H), red; bulk O(H), gray; and O of bulk H_2O, dark blue.).

hydrogen-bonded interactions with the surface (hydr)oxo groups. The second and third gas-side water layers that were structurally similar to those of their liquid water counterparts form, however, at greater water loading. We also note the presence of an additional water species that is present at the tunnel entrances just 0.19 nm below the geminal waters. This species is stabilized by two accepting and two donating hydrogen bonds with vicinal surface hydroxo groups (Figure 5) and is a precursor to those diffusing through the akaganéite bulk.

Extended (>600 ns) simulations revealed a two-stage diffusion process to the akaganéite bulk (Figure 6a). A relatively rapid water uptake that is associated with a drop in the total energy of the system occurred within 100 ns and was followed by a considerably more sluggish uptake with time (Figure 6a). A density profile of the akaganéite/water interface (Figure 6b) revealed increasing densities of water within the first three top bulk cavities for water within this time scale, even though the preferential accumulation of water will first occur on the gas side of the mineral/gas interface. These sluggish diffusion reactions were caused by the extensive interactions that take place between the water and bulk hydroxo groups, as will now be detailed.

MD simulations of a bulk akaganéite cell (no interface) containing fixed quantities of Cl^- and H_2O provided further insight into the nature of the molecular interactions that generated the FTIR spectral features found in Figure 4. The results of these simulations were compared to those of simulation cells with empty tunnels as well as other cells

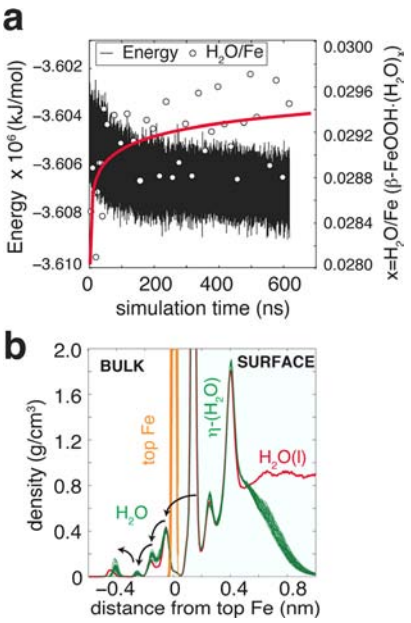

Figure 6. Time-resolved energy of the $Fe_{1664}O_{1152}(OH)_{1920}Cl_{202}(H_2O)_{800}$ supercell upon exposing the (010) plane to gaseous water and the corresponding bulk-H_2O/Fe ratios obtained by MD (1 fs time step, 300 K, NPT) (a). The latter values were obtained as the average time of 20 ns segments of this ~600 ns simulation for all of the bulk waters located behind the surface Fe atoms. Density profiles of the akaganéite/water interface obtained from the same 20 ns segments (b).

containing only Cl^- or H_2O. The resulting theoretical power spectra (Figure 7) that were generated from these simulations

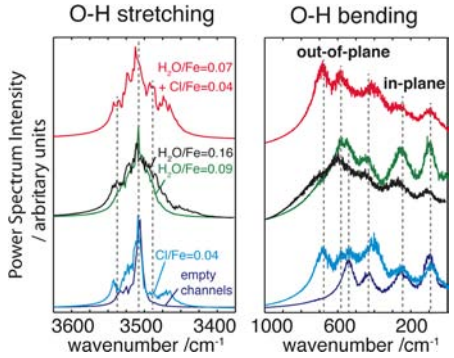

Figure 7. Power spectra obtained from the Fourier transform of the hydrogen autocorrelation function of 50 ps MD simulations (1 as time step, 300 K, NPT, no LINCS on O−H) for the $Fe_{1792}O_{1792}(OH)_{1792}$, $Fe_{1792}O_{1392}(OH)_{2192}Cl_{210}$, and $Fe_{1792}O_{1652}(OH)_{1932}Cl_{73}$ supercells. The O−H stretching region is shown on the left, and the bending region is shown on the right.

show that the addition of water to an ion- and water-free akaganéite lattice broadens the bulk O−H stretching vibrations, thereby effectively decreasing the intensities at their bulk sorption maximum. The addition of Cl^- further broadens and red shifts the O−H stretching frequencies by forming hydrogen bonds, thus further affecting the interactions between the bulk OH and water. The power spectra show that, in keeping with the experimental spectra, both H_2O and Cl^- strengthen the in-plane and restrict the out-of-plane bending modes. The concurrence of these theoretical spectral features with those

dx.doi.org/10.1021/ic400661d | Inorg. Chem. 2013, 52, 7107−7113

seen in the laboratory thus reinforces our interpretations for water diffusion reactions to the akaganéite bulk.

These interactions can be further resolved through bonding and dynamics analysis. The bonding analysis first confirmed that both Cl^- and H_2O lie at the center of a cubic cavity that is defined by eight OH groups (Figure 1). This was specifically seen in the cumulative coordination numbers that were computed from radial distribution functions for the various possible interactions (Figure S4). Cl−OH interactions almost exclusively involve eight OH groups, with a median Cl−O distance of 0.22 nm, and contribute to the small diffusion coefficient ($D = 9.2 \times 10^{-13}$ $m^2 \cdot s^{-1}$) of this ion in the tunnels. Note, however, that the immobility of the protons in our simulations, caused by the imposed harmonic O−H bond, may also be a contributing factor to these small values.

Interactions between the bulk OH and water were relatively more convoluted. The geometric analysis of these interactions (SI, section 2) leads us to classify them as hydrogen bonds, yet their populations exceeded the number of donating and accepting bonds that are typically formed by water. The population analysis suggests the existence of three dominant configurations (Figures 1c and S5) that involve a total of 10 (i.e., 3.33 per H_2O per configuration) accepting bonds from OH groups, four (i.e., 1.33 per H_2O per configuration) donating bonds to OH groups, and one-half (i.e., 0.16 per H_2O per configuration) donating bonds to O groups. Note that these configurations are short-lived and therefore explain the overbonding. The approximate half-lives for these bonds (Figure S6) are, in fact, less than 0.5 ps, a value that is substantially smaller than that of strongly hydrogen-bonded systems such as those in the FeOOH/water interface.[37] Furthermore, these interactions are responsible for the considerably small diffusion coefficients ($D = 4.1-11.1 \times 10^{-12}$ $m^2 \cdot s^{-1}$) and integral rotational correlation time ($\tau_r = 8.4-24.7$ ps) of bulk water, especially when compared to those of liquid water ($D = 2.8 \times 10^{-9}$ $m^2 \cdot s^{-1}$; $\tau_r = 2$ ps; note that we also reproduced these literature values).[52] These parameters are highly correlated with bulk water loading (Figure 8), revealing

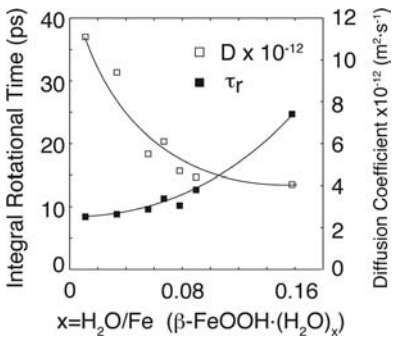

Figure 8. Integral rotational correlation time (τ_r) and diffusion coefficient (D) as a function of bulk water loading obtained by an MD simulation of the $Fe_{1792}O_{1792}(OH)_{1792}$ supercell (5 ns simulation, 0.5 ps time step, 300 K, NPT).

that the previously immobile waters in the dehydrated akaganéite bulk can be of varied mobility and rotatability, albeit to an extent that is nothing compared to that of liquid water or even compared to the greatest loading that was considered in this work. Finally, these simulations also revealed interactions between Cl^- and H_2O from adjacent cavities with an average Cl−O_w (Cl−H_w) bonding distance of 0.34 nm (0.24 nm), about 0.02 nm longer than in aqueous solutions (Figure S4). Such interactions, which were notably considered by Zhu and Kubicki,[53] should predominate in water-laden structures. In summary, these analyses point to high degrees of interactions between water and bulk (hydr)oxo groups and to sluggish diffusion rates that can lead to significant levels of bulk water molecules in akaganéite nanoparticles.

4. CONCLUSIONS

The substantial network of hydrogen bonding environments of the water molecules in the akaganéite bulk is an important contributing factor to the water-diffusion rates in this material. This was underscored by MD simulations, pointing to high degrees of bonding coupled with fast rates of bond forming and breaking. Important differences should, however, be noted between our simulations and those of the laboratory experiments. First, the time scale of the simulations is orders of magnitude smaller in comparison to that of the laboratory reaction times (20 min) despite efforts to prolong the simulations beyond 600 ns. Second, defects in the synthesized particles contributed to the water uptake that was observed in the laboratory, in contrast to simulations where only idealized structures were considered. Therefore, although bulk protons and chloride were immobile during the course of a simulation, the exchange of HCl for water, especially at high liquid waterlike loading, is certainly a possibility in the time scale of our experiments.

This work presents experimental and theoretical evidence for water molecule diffusion into the tunnel structure of akaganéite. The bulk water molecules induce important changes in the hydrogen bonding environment of the bulk hydroxyls and can be present in loadings of up to 22.4 mg/g akaganéite. This level of water occupation affects the physicochemical attributes of this material and should therefore be considered in any system where akaganéite particles are in contact with either liquid or gaseous water.

■ ASSOCIATED CONTENT

Supporting Information

Akaganéite synthesis and characterization. Detailed methods and discussions of molecular dynamics simulations. This material is available free of charge via the Internet at http://pubs.acs.org.

■ AUTHOR INFORMATION

Corresponding Author

*E-mail: xiaowei.song@chem.umu.se. Phone: +46 90 786 5361.

Notes

The authors declare no competing financial interest.

■ ACKNOWLEDGMENTS

This work was supported by the Swedish Research Council (2009-3110, 2012-2976), the Knut and Alice Wallenberg Foundation, the J.C. Kempe Foundation, and the Carl Tryggers Foundation.

■ REFERENCES

(1) Post, J. E.; Heaney, P. J.; Von Dreele, R. B.; Hanson, J. C. *Am. Mineral.* **2003**, *88* (5−6), 782−788.

(2) Schwertmann, U.; Cornell, R. M.*The Iron Oxides: Structure, Properties, Reactions, Occurrences and Uses*; Wiley-VCH: Weinheim, Germany, 2003.

(3) Ståhl, K.; Nielsen, K.; Jiang, J. Z.; Lebech, B.; Hanson, J. C.; Norby, P.; van Lanschot, J. *Corros. Sci.* **2003**, *45* (11), 2563−2575.
(4) Cai, J.; Liu, J.; Gao, Z.; Navrotsky, A.; Suib, S. L. *Chem. Mater.* **2001**, *13* (12), 4595−4602.
(5) Mazeina, L.; Deore, S.; Navrotsky, A. *Chem. Mater.* **2006**, *18* (7), 1830−1838.
(6) Yue, J.; Jiang, X. C.; Yu, A. B. *J. Nanopart. Res.* **2011**, *13* (9), 3961−3974.
(7) Holm, N. G.; Dowler, M. J.; Wadsten, T.; Arrhenius, G. *Geochim. Cosmochim. Acta* **1983**, *47* (8), 1465−1470.
(8) Johnston, J. H. *Geochim. Cosmochim. Acta* **1977**, *41* (4), 539−544.
(9) Logan, N. E.; Johnston, J. H.; Childs, C. W. *Aust. J. Soil Res.* **1976**, *14* (2), 217−224.
(10) Anthony, J. W.; Bideaux, R. A.; Bladh, K. W.; Nichols, M. C. *Handbook of Mineralogy*; Mineralogical Society of America: Chantilly, VA, 2001.
(11) Hodges, R. R. *J. Geophys. Res.* 2002, *107* (E2), 5011−5017.
(12) Taylor, L. A.; Mao, H. K.; Bell, P. M. *Geology* **1974**, *2* (9), 429−432.
(13) Fleischer, I.; Schröder, C.; KlingelhöFer, G.; Zipfel, J.; Morris, R. V.; Ashley, J. W.; Gellert, R.; Wehrheim, S.; Ebert, S. *Meteorit. Planet. Sci.* **2011**, *46* (1), 21−34.
(14) Glotch, T. D.; Rossman, G. R. *Icarus* **2009**, *204* (2), 663−671.
(15) Schröder, C.; Rodionov, D. S.; McCoy, T. J.; Jolliff, B. L.; Gellert, R.; Nittler, L. R.; Farrand, W. H.; Johnson, J. R.; Ruff, S. W.; Ashley, J. W.; Mittlefehldt, D. W.; Herkenhoff, K. E.; Fleischer, I.; Haldemann, A. F. C.; Klingelhöfer, G.; Ming, D. W.; Morris, R. V.; de Souza, P. A.; Squyres, S. W.; Weitz, C.; Yen, A. S.; Zipfel, J.; Economou, T., *J. Geophys. Res.* 2008, *113* (E6), E06S22.
(16) Zalutskii, A. A.; Ivanov, A. V.; Morozov, V. V.; Sed'mov, N. A.; Shoba, S. A. *Dokl. Earth Sci.* **2011**, *441* (1), 1526−1528.
(17) Perez, F. R.; Barrero, C. A.; Garcia, K. E. *Corros. Sci.* **2010**, *52* (8), 2582−2591.
(18) Zou, Y.; Wang, J.; Zheng, Y. Y. *Corros. Sci.* **2011**, *53* (1), 208−216.
(19) Xu, C. H.; Shi, J. J.; Zhou, W. Z.; Gao, B. Y.; Yue, Q. Y.; Wang, X. H. *Chem. Eng. J.* **2012**, *187*, 63−68.
(20) Chitrakar, R.; Makita, Y.; Sonoda, A. *Chem. Lett.* **2012**, *41* (12), 1694−1696.
(21) Kyzas, G. Z.; Peleka, E. N.; Deliyanni, E. A. *Materials* **2013**, *6* (1), 184−197.
(22) Tabuchi, T.; Katayama, Y.; Nukuda, T.; Ogumi, Z. *J. Power Sources* **2009**, *191* (2), 636−639.
(23) Tabuchi, T.; Katayama, Y.; Nukuda, T.; Ogumi, Z. *J. Power Sources* **2009**, *191* (2), 640−643.
(24) Wu, P. C.; Wang, W. S.; Huang, Y. T.; Sheu, H. S.; Lo, Y. W.; Tsai, T. L.; Shieh, D. B.; Yeh, C. S. *Chem.—Eur. J.* **2007**, *13* (14), 3878−3885.
(25) Garcia, K. E.; Morales, A. L.; Barrero, C. A.; Arroyave, C. E.; Greneche, J. M. *Physica B* **2004**, *354* (1−4), 187−190.
(26) Song, X. W.; Boily, J. F. *J. Phys. Chem. C* **2012**, *116* (3), 2303−2312.
(27) Song, X. W.; Boily, J. F. *J. Colloid Interface Sci.* **2012**, *376*, 331−333.
(28) Mulababafubiandi, A.; Helsen, J. A.; Paterson, R.; Langouche, G. *Hyperfine Interact.* **1990**, *56* (1−4), 1701−1706.
(29) Marcus, Y. *Chem. Rev.* **1988**, *88* (8), 1475−1498.
(30) Liu, X.-M.; Fu, S.-Y.; Xiao, H.-M.; Huang, C.-J. *J. Solid State Chem.* **2005**, *178* (9), 2798−2803.
(31) Yuan, Z.-Y.; Su, B.-L. *Chem. Phys. Lett.* **2003**, *381* (5−6), 710−714.
(32) Felix, F.*Water: A Matrix of Life*; The Royal Society of Chemistry: Cambridge, U.K., 2000.
(33) Osterloo, M. M.; Hamilton, V. E.; Bandfield, J. L.; Glotch, T. D.; Baldridge, A. M.; Christensen, P. R.; Tornabene, L. L.; Anderson, F. S. *Science* **2008**, *319* (5870), 1651−1654.
(34) Cornell, R. M.; Schwertmann, U. *Iron Oxides in the Laboratory*; Wiley-VCH: Weinheim, Germany, 1991.
(35) Song, X. W.; Boily, J. F. *J. Phys. Chem. C* **2011**, *115* (34), 17036−17045.
(36) Song, X. W.; Boily, J. F. *Phys. Chem. Chem. Phys.* **2012**, *14* (8), 2579−2586.
(37) Song, X. W.; Boily, J. F. *Chem. Phys. Lett.* **2013**, *560* (0), 1−9.
(38) Golub, G. H.; Reinsch, C. *Numer. Math.* **1970**, *14* (5), 403−420.
(39) Sauerbrey, G. *Z. Phys.* **1959**, *155* (2), 206−222.
(40) Do, D. D.; Do, H. D. *Carbon* **2000**, *38* (5), 767−773.
(41) Venema, P.; Hiemstra, T.; Weidler, P. G.; van Riemsdijk, W. H. *J. Colloid Interface Sci.* **1998**, *198* (2), 282−295.
(42) Kozin, P. A.; Boily, J.-F. *J. Phys. Chem. C* **2013**, *117* (12), 6409−6419.
(43) Cygan, R. T.; Liang, J. J.; Kalinichev, A. G. *J. Phys. Chem. B* **2004**, *108* (4), 1255−1266.
(44) Teleman, O.; Jonsson, B.; Engstrom, S. *Mol. Phys.* **1987**, *60* (1), 193−203.
(45) Hockney, R. W.; Goel, S. P.; Eastwood, J. W. *J. Comput. Phys.* **1974**, *14* (2), 148−158.
(46) Nose, S.; Klein, M. L. *Mol. Phys.* **1983**, *50* (5), 1055−1076.
(47) Parrinello, M.; Rahman, A. *J. Appl. Phys.* **1981**, *52* (12), 7182−7190.
(48) Hess, B.; Bekker, H.; Berendsen, H. J. C.; Fraaije, J. *J. Comput. Chem.* **1997**, *18* (12), 1463−1472.
(49) Darden, T.; York, D.; Pedersen, L. *J. Chem. Phys.* **1993**, *98* (12), 10089−10092.
(50) Essmann, U.; Perera, L.; Berkowitz, M. L.; Darden, T.; Lee, H.; Pedersen, L. G. *J. Chem. Phys.* **1995**, *103* (19), 8577−8593.
(51) van der Spoel, D.; Lindahl, E.; Hess, B.; Groenhof, G.; Mark, A. E.; Berendsen, H. J. C. *J. Comput. Chem.* **2005**, *26* (16), 1701−1718.
(52) van der Spoel, D.; van Maaren, P. J.; Berendsen, H. J. C. *J. Chem. Phys.* **1998**, *108* (24), 10220.
(53) Zhu, Q.; K., P.; Heaney, P.; Ilott, A.; Phillips, B.; Adri van Duin, V. A.; Kubicki, J. *DFT and Reactive Force Field Studies of β-FeOOH*. 243rd ACS National Meeting and Exposition, San Diego, CA, March 25−29, 2012; American Chemical Society: Washington, DC, 1996.